Stable Second-Order Explicit Runge-Kutta Finite Difference Time Domain Formulations for Modeling Graphene Nano-Material Structures

Omar Ramadan

Abstract In this paper, stable second-order Runge-Kutta finite difference time domain (RK-FDTD) formulations are introduced for modeling graphene nano-material structures. In this respect, a differencing scheme in which the electric field and the associated current density are collocated in time and space is used for incorporating graphene's dispersion into the FDTD algorithm. The stability of the formulations is studied by using the root-locus method, and it is shown that the given formulations maintain the conventional Courant-Friedrichs-Lewy (CFL) time-step stability limit. The stability and the accuracy of the formulations are validated through a numerical test that investigates the tunneling phenomena of electromagnetic wave propagation through an infinite free-standing graphene layer.

Keywords Explicit finite difference time domain (FDTD) · Auxiliary differential equation (ADE) · Root-locus stability analysis · Second-order Runge-Kutta (RK) scheme · Graphene nano-material

1 Introduction

Graphene nano-material has attracted tremendous attention due to its exceptional electrical, optical, and mechanical properties [1], and this increases the interest of developing accurate and efficient numerical techniques for modeling graphene structures. In the last two decades, the finite difference time domain (FDTD) method [2], which is known to be one of the most popular electromagnetic time domain numerical techniques, has been widely used in graphene simulations [3–5]. In these approaches, the auxiliary differential equation method is used for incorporating graphene's dispersion into the FDTD algorithm.

In this paper, alternative formulations based on combining the second- order Runge-Kutta scheme [6] with the FDTD algorithm are introduced for model graphene

O. Ramadan (✉)
Computer Engineering Department, Eastern Mediterranean University, Gazimagusa, Mersin 10, Turkey
e-mail: omar.ramadan@emu.edu.tr

D. Zeidan et al. (eds.), *Mathematics and Computation*, Springer Proceedings in Mathematics & Statistics 418, https://doi.org/10.1007/978-981-99-0447-1_13

structures. In this respect, a differencing scheme in which the electric field and the associated current density are collocated in time and space is used for incorporating graphene's dispersion into the FDTD algorithm. The stability of the formulations is studied by using the root-locus method [7], and it is shown that the given formulations maintain the conventional Courant-Friedrichs-Lewy (CFL) time-step stability limit. The stability and accuracy of the formulations are validated through a numerical test that investigates the tunneling phenomena of electromagnetic wave propagation through an infinite free-standing graphene layer.

2 Formulations

At microwave and THz frequency regimes, the surface conductivity of graphene can be written as [8]

$$\sigma_{\mathtt{intra}} = \frac{\sigma_0}{\mathbf{j}\omega + v} \tag{1}$$

where v is the scattering rate, and $\sigma_0 = e^2 k_B T \left(\frac{\mu_c}{k_B T} + 2\ln(e^{-\mu_c/k_B T} + 1) \right) / \pi\hbar^2$ is the static conductivity, where $-e$ is the electron charge, k_B is Boltzmann's constant, T is the temperature, μ_c is the chemical potential, and $\hbar$ is the reduced Planck's constant. Considering a graphene layer of thickness D_g, and introducing the concept of volumetric conductivity $\sigma_v = \sigma_{\mathtt{intra}}/D_g$ [9], the equations for the electric field component E_η, $(\eta = x, y, z)$, and the associated current density J_η can be written as

$$\varepsilon_0 \frac{\partial E_\eta}{\partial t} = \nabla \times \mathbf{H}|_\eta - \frac{1}{D_g} J_\eta \tag{2}$$

$$\frac{\partial J_\eta}{\partial t} = \sigma_0 E_\eta - v J_\eta \tag{3}$$

Letting the electric field and the associated current density be collocated in time and space, (2) can be discretized as

$$\varepsilon_0 \frac{\delta_t}{\Delta_t} E_\eta \big|_{r_{Ex}}^{n+\frac{1}{2}} = \widetilde{\nabla} \times \mathbf{H}\big|_{\eta_{r_{E\eta}}}^{n+\frac{1}{2}} - \frac{1}{D_g} \mu_t \, J_\eta \big|_{r_{Ex}}^{n+\frac{1}{2}} \tag{4}$$

where $r_{E\eta}$ is the spatial position of E_η, Δ_t is the time step, $\Psi^n = \Psi^n(n\Delta_t)$ $(\Psi = E, H, J)$, δ_t is the centered temporal difference operator given by

$$\delta_t u^q_{\alpha,\beta,\gamma} = u^{q+\frac{1}{2}}_{\alpha,\beta,\gamma} - u^{q-\frac{1}{2}}_{\alpha,\beta,\gamma} \tag{5}$$

where $u^q_{\alpha,\beta,\gamma} = u\,(q\Delta_t,\ \alpha\Delta_x,\ \beta\Delta_x,\ \gamma\Delta_z)$, with $q = \left\{n,\ n+\frac{1}{2}\right\}$, $\alpha = \left\{i,\ i+\frac{1}{2}\right\}$, $\beta = \left\{j,\ j+\frac{1}{2}\right\}$, and $\gamma = \left\{k,\ k+\frac{1}{2}\right\}$, μ_t is the discrete averaging operator defined as

$$\mu_t u^q_{\alpha,\beta,\gamma} = \frac{u^{q+\frac{1}{2}}_{\alpha,\beta,\gamma} + u^{q+\frac{1}{2}}_{\alpha,\beta,\gamma}}{2} \tag{6}$$

and, finally, $\widetilde{\nabla}\times$ is the discrete version of $\nabla\times$ given by

$$\widetilde{\nabla}\times = \begin{pmatrix} 0 & -\delta_z & \delta_y \\ \delta_z & 0 & -\delta_x \\ -\delta_y & \delta_x & 0 \end{pmatrix} \tag{7}$$

where $\delta_\eta, \eta \in \{x,\ y,\ z\}$, is the centered spatial difference operator in the η-coordinate, for instance, δ_x is defined at the $(\alpha,\ \beta,\ \gamma)$ grid position as

$$\delta_x u^q_{\alpha,\beta,\gamma} = \frac{u^q_{\alpha+\frac{1}{2},\beta,\gamma} - u^q_{\alpha-\frac{1}{2},\beta,\gamma}}{\Delta_x} \tag{8}$$

with Δ_x being the mesh size along the x-coordinate. Based on (4), the E_η electric field component can be approximated at $n+1$ time step as

$$E^{n+1}_{\eta_{rE\eta}} = E^n_{\eta_{rE\eta}} + \frac{\Delta_t}{\varepsilon_0}\,\widetilde{\nabla}\times \mathbf{H}\Big|^{n+\frac{1}{2}}_{\eta_{rE\eta}} - \frac{\Delta_t}{2\varepsilon_0 D_g}\left(J^{n+1}_{\eta_{rE\eta}} + J^n_{\eta_{rE\eta}}\right) \tag{9}$$

By employing the general second-order RK [6] scheme to (3), J^{n+1}_η can be approximated as

$$\begin{cases} \mathcal{K}_1 = \Delta_t f\left(n\Delta_t,\ J^n_\eta\right) \\ \mathcal{K}_2 = \Delta_t f\left((n+\lambda_1)\,\Delta_t,\ J^n_\eta + \lambda_2\mathcal{K}_1\right) \\ J^{n+1}_\eta = J^n_\eta + a_1\mathcal{K}_1 + a_2\mathcal{K}_2 \end{cases} \tag{10}$$

where f is obtained from the right-hand side of (3) as

$$f = \sigma_0 E_\eta - v J_\eta \tag{11}$$

and

$$\begin{cases} a_1 + a_2 = 1 \\ \lambda_1 a_2 = \frac{1}{2} \\ \lambda_2 a_2 = \frac{1}{2} \end{cases} \tag{12}$$

It is important to note that the approximation of (10) is of second-order accuracy, as shown in the Appendix. Employing the midpoint integration rule [6], which is also known as the modified Euler method, these constants can be obtained as

$$a_1 = 0,\ a_2 = 1,\ \text{and}\ \lambda_1 = \lambda_2 = \frac{1}{2} \tag{13}$$

Hence, J_η^{n+1} can be re-arranged from (10) as

$$J_\eta^{n+1} = J_\eta^n + \Delta_t f\left(\left(n+\frac{1}{2}\right)\Delta_t,\ J_\eta^n + \frac{\Delta_t}{2} f\left(n\Delta_t + J_\eta^n\right)\right) \tag{14}$$

which can be written recursively at the $r_{E\eta}$ grid position as

$$J_{\eta_{r_{E\eta}}}^{n+1} = b_1 J_{\eta_{r_{E\eta}}}^n + b_2 E_{\eta_{r_{E\eta}}}^n \tag{15}$$

where $b_1 = 1 - \tilde{v} + \frac{\tilde{v}^2}{2}$ and $b_2 = \sigma_0 \tilde{v}\left(1 - \frac{\tilde{v}}{2}\right)$ with $\tilde{v} = v\Delta_t$. For completeness, the magnetic field component H_η is written in the FDTD form as [2]

$$H_{\eta_{r_{H\eta}}}^{n+\frac{1}{2}} = H_{\eta_{r_{H\eta}}}^{n-\frac{1}{2}} - \frac{\Delta_t}{\mu_0}\,\widetilde{\nabla} \times \mathbf{E}\big|_{\eta_{r_{H\eta}}}^n \tag{16}$$

In the following section, the stability analysis of the above formulations is investigated by using the root-locus method [7].

3 Root-Locus Stability Analysis

Let the time-harmonic solution of the above field equations with the variables E, H, and J be given by

$$\Psi_{\alpha,\beta,\gamma}^n = \Psi_0 e^{\mathbf{j}\left(\omega n\Delta_t - \widetilde{k}_x \alpha\Delta_x - \widetilde{k}_y \beta\Delta_y - \widetilde{k}_z \gamma\Delta_z\right)} \tag{17}$$

where $\mathbf{j} = \sqrt{-1}$, $\Psi_{\alpha,\beta,\gamma}^n = \Psi\left(n\Delta_t,\ \alpha\Delta_x,\ \beta\Delta_y,\ \gamma\Delta_z\right)$, Ψ_0 is the complex amplitude of the field Ψ, and $\widetilde{k}_\eta$ $(\eta = x,\ y,\ z)$ is the wave number in the discrete mode along the η-direction. Upon substituting (17) into (9), (14), and (16), the following system can be obtained:

$$\begin{bmatrix} (\mathcal{Z}-b_1)\,\mathbf{I}_3 & -b_2\mathbf{I}_3 & \mathbf{0}_3 \\ \frac{\Delta_t(\mathcal{Z}+1)}{2\varepsilon_0 D_g}\mathbf{I}_3 & (\mathcal{Z}-1)\,\mathbf{I}_3 & \frac{\Delta_t \mathcal{Z}^{\frac{1}{2}}}{\varepsilon_0}\mathcal{C} \\ \mathbf{0}_3 & \frac{\Delta_t}{\mu_0}\mathcal{C}^T & \left(\mathcal{Z}^{\frac{1}{2}} - \mathcal{Z}^{-\frac{1}{2}}\right)\mathbf{I}_3 \end{bmatrix} \times \begin{bmatrix} \mathbf{J}_0 \\ \mathbf{E}_0 \\ \mathbf{H}_0 \end{bmatrix} = 0 \tag{18}$$

where $\mathcal{Z} = e^{j\omega\Delta_t}$ is the stability factor, $\mathbf{0}_3$ is a 3×3 null matrix, $\mathbf{I}_3$ is a 3×3 identity matrix, and $\mathcal{C}$ contains the eigenvalues of the curl operator of Maxwell's equations given by

$$\mathcal{C} = \begin{pmatrix} 0 & \widehat{\delta}_z & -\widehat{\delta}_y \\ -\widehat{\delta}_z & 0 & \widehat{\delta}_x \\ \widehat{\delta}_y & -\widehat{\delta}_x & 0 \end{pmatrix} \tag{19}$$

where $\widehat{\delta}_\eta = \mathbf{j}2\sin\left(k_\eta\Delta_\eta/2\right)/\Delta_\eta$. Equating the determinant of the coefficient matrix of (18) to zero and taking $\sin\left(\widetilde{k}_\eta\Delta_\eta/2\right) = 1$, to account for the worst possible case, the presented explicit RK-FDTD scheme will have the following stability polynomial:

$$\left(\frac{\mathcal{Z}-1}{\mathcal{Z}^{\frac{1}{2}}}\right)\left(\frac{\mathcal{Z}-b_1}{\mathcal{Z}^{\frac{1}{2}}}\right)^2 \left[(\mathcal{Z}-b_1)(\mathcal{Z}-1) + \frac{b_2\Delta_t}{2\varepsilon_0 D_g}(\mathcal{Z}+1)\right]\left(S^{\mathcal{RK}}(\mathcal{Z})\right)^2 = 0 \tag{20}$$

where $S^{\mathcal{RK}}(\mathcal{Z})$ is given by

$$S^{\mathcal{RK}}(\mathcal{Z}) = 4\mathcal{CN}^2\mathcal{Z} + (\mathcal{Z}-1)^2 + \frac{b_2\Delta_t}{2\varepsilon_0 D_g}\frac{(\mathcal{Z}+1)(\mathcal{Z}-1)}{(\mathcal{Z}-b_1)} \tag{21}$$

and $\mathcal{CN}$ is the Courant number defined as

$$\mathcal{CN} = \frac{\Delta_t}{\Delta_{t_{\max}}^{\mathcal{CFL}}} \tag{22}$$

with $\Delta_{t_{\max}}^{\mathcal{CFL}} = 1/c_0\sqrt{\Delta_x^{-2} + \Delta_y^{-2} + \Delta_z^{-2}}$ being the CFL time-step limit [2], and $c_0 = 1/\sqrt{\varepsilon_0\mu_0}$ being the speed of light in free space. Based on (20) and (21), a reduced stability can be re-arranged from (21) as

$$1 + 4\mathcal{CN}^2\frac{\mathcal{Z}}{(\mathcal{Z}-1)^2}\frac{1}{\widetilde{\varepsilon}_r^{\mathcal{RK}}(\mathcal{Z})} = 0 \tag{23}$$

where $\widetilde{\varepsilon}_r^{\mathcal{RK}}(\mathcal{Z})$ is the numerical permittivity of the presented explicit RK-FDTD scheme, which can be arranged as

$$\widetilde{\varepsilon}_r^{\mathcal{RK}}(\mathcal{Z}) = 1 + \frac{b_2\Delta_t}{2\varepsilon_0 D_g}\frac{(\mathcal{Z}+1)}{(\mathcal{Z}-1)(\mathcal{Z}-b_1)} \tag{24}$$

Based on the root-locus stability analysis [7], the maximum time step of the presented RK-FDTD implementation $\left(\Delta_{t_{\max}}^{\mathcal{RK}}\right)$ can be obtained from the fact that the roots of (23) must lie inside or on the unit circle in the $\mathcal{Z}$-plane, i.e., $|\mathcal{Z}| \leq 1$. To better

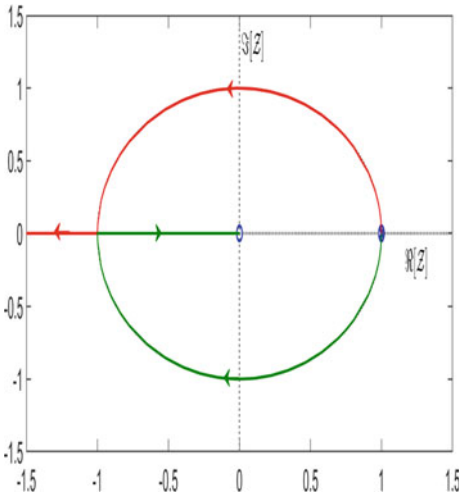

Fig. 1 Root-locus of (23) for the presented explicit RK-FDTD implementation. Graphene parameters are taken as $\upsilon = 2.0$ THz, $\mu_c = 1.0$ eV, $T = 300$ Kelvin, and $d = \Delta = c_0/200\, f_{\max}$, with $f_{\max} = 10$ THz

visualize this idea, consider a graphene layer with the following parameters: $\upsilon = 2.0$ THz, $\mu_c = 1.0$ eV, $T = 300$ Kelvin, and let the graphene layer occupy one spatial cell [10], i.e., $D_g = \Delta$, where $\Delta = \Delta_x = \Delta_y = \Delta_z = c_0/200\, f_{\max}$ with $f_{\max} = 10$ THz. Figure 1 shows the root-locus of (23), where the initial time step is taken to satisfy $\Delta_{t_{\max}}^{\mathcal{CFL}}$ [11]. As can be seen from Fig. 1, the instability occurs at $\mathcal{Z} = -1$. Hence, by substituting $\mathcal{Z} = -1$ into (23) together with (24) the following can be obtained:

$$1 - \mathcal{CN}^2 = 0 \tag{25}$$

and this implies that $\mathcal{CN}$ is always unity for the presented RK-FDTD scheme and independent from graphene parameters. Noting that $\mathcal{CN} = \Delta_t / \Delta_{t_{\max}}^{\mathcal{CFL}}$, the time-step constraint for the explicit RK-FDTD scheme $\left(\Delta_{t_{\max}}^{\mathcal{RK}}\right)$ can be obtained from (25) as

$$\Delta_{t_{\max}}^{\mathcal{RK}} = \Delta_{t_{\max}}^{\mathcal{CFL}} \tag{26}$$

Hence, the presented RK-FDTD scheme retains $\Delta_t^{\mathcal{CFL}}$.

4 Numerical Stability and Accuracy Verification

In this section, the stability and accuracy of the presented explicit RK-FDTD scheme are verified through a numerical test that investigates electromagnetic wave propagation through an infinite free-standing graphene layer. For this purpose, an electromagnetic wave with E_z and H_y field components propagating in a one-dimensional (1-D) domain along the x-direction is considered. The size of the simulation domain is taken as $8000\Delta_x$, where $\Delta_x = c_0/200\, f_{\max}$ and $f_{\max} = 10$ THz. The convolutional

perfectly matched layer (CPML) [12], with a thickness of 10 cells, is used to truncate the computational domain. The graphene layer, with the same parameters used for Fig. 1, occupies one spatial cell at grid point 4000. The simulation domain geometry is shown in Fig. 2. The excitation is a Gaussian pulse with a time dependence of

$$g(t) = e^{-4\pi(t-t_d)^2/t_w^2} \tag{27}$$

where $t_w = 80\Delta_t$ and $t_d = 6t_w$. The excitation source is located at point **S**, and the observation point is located at point **O**, as shown in Fig. 2. The simulation is conducted for the first 100 000 time steps. Figure 3 shows the transmitted E_z field recorded at the observation point **O**, $\left(E_z^{tr}\,(4020\Delta_x)\right)$, computed by the presented explicit RK-FDTD implementation with $\Delta_t = \Delta_{t_{\max}}^{\mathcal{RK}} = \Delta_{t_{\max}}^{\mathcal{CFL}}$. Clearly, E_z remains stable over the complete simulation time and, therefore, the stability of the presented explicit RK-FDTD implementation maintains the conventional time-step CFL constraint. It must be noted that the simulation is also conducted with the presented explicit RK-FDTD implementation for the first 1×10^6 time steps and no instability is observed.

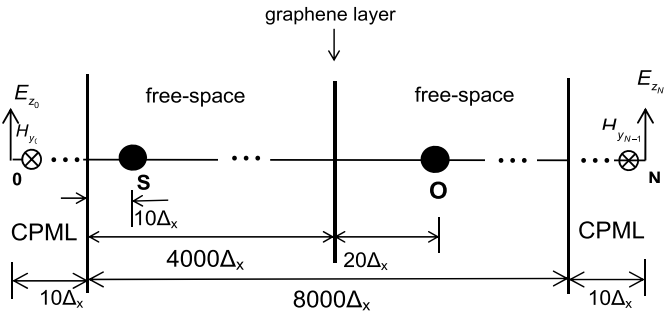

Fig. 2 One-dimensional simulation domain geometry

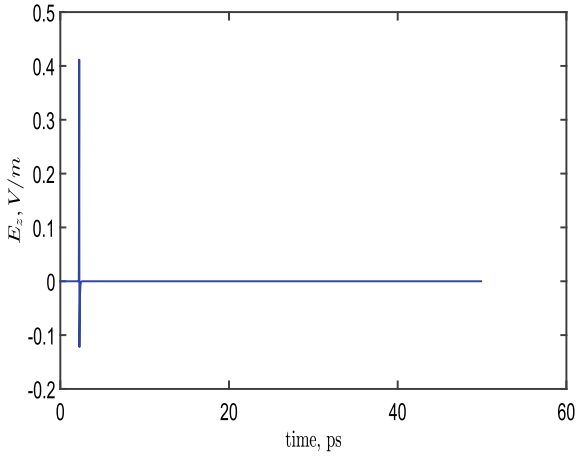

Fig. 3 Transmitted electric field at node 4020, $E_z^{tr}\,(4020\Delta_x)$ computed by the presented explicit RK-FDTD with $\Delta_t = \Delta_{t_{\max}}^{\mathcal{RK}} = \Delta_{t_{\max}}^{\mathcal{CFL}}$

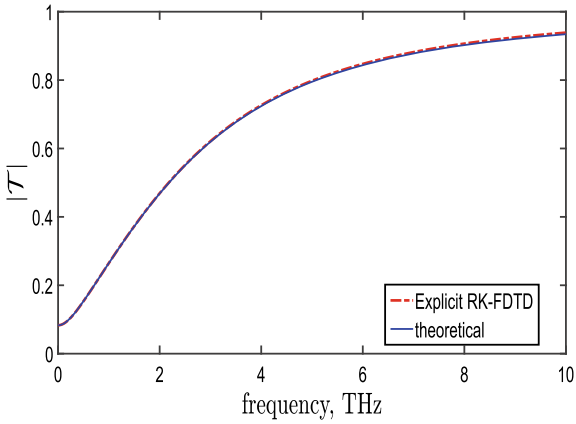

Fig. 4 Transmission coefficient magnitude for a graphene layer computed by the presented explicit RK-FDTD, and the theoretical approaches

Finally, the accuracy of the presented explicit RK-FDTD implementations is studied. For this purpose, the transmission coefficient ($\mathcal{T}$) of the graphene layer is investigated and computed as

$$\mathcal{T}(\omega) = \frac{E_z^{tr}(\omega)}{E_z^{inc}(\omega)} \tag{28}$$

where $E_z^{tr}(\omega)$ is the frequency domain of the transmitted field E_z^{tr}, and $E_z^{inc}(\omega)$ is frequency domain of the incident field E_z^{inc} recorded at the observation point $\mathbf{O}$, which is obtained in the second simulation by replacing the graphene layer with vacuum. Figure 4 shows the magnitude of the transmission coefficient for the presented explicit RK-FDTD scheme with $\Delta_t = \Delta_{t_{\max}}^{\mathcal{RK}} = \Delta_{t_{\max}}^{\mathcal{CFL}}$. Figure 4 shows also the magnitude of the theoretical transmission coefficient ($\mathcal{T}_{th}$) [8]. Clearly, both schemes give high accuracy as the theoretical results.

5 Conclusions

In this paper, stable and accurate Runge-Kutta FDTD formulations are presented for graphene simulations. It is shown that the presented formulations not only retain the standard CFL time-step stability limit but also exhibit high accuracy as compared with the theoretical results.

6 Appendix: Runge-Kutta Local Truncation Error

Considering $\mathcal{K}_2 = \Delta_t f\left((n+\lambda_1)\,\Delta_t,\, J_\eta^n + \lambda_2 \mathcal{K}_1\right)$ given in (10), and applying the multivariate Taylor series expansion, the following can be obtained:

$$\begin{aligned}\mathcal{K}_2 = \Delta_t \Big[& f\left(n\Delta_t + J_\eta^n\right) + \lambda_1 \Delta_t f_t'\left(n\Delta,\, J_\eta^n\right) \\ & + \lambda_2 \mathcal{K}_1 f_{J_\eta}'\left(n\Delta,\, J_\eta^n\right) + O\left(\Delta_t^2,\, \mathcal{K}_1^2\right)\Big]\end{aligned} \tag{29}$$

where f_t' and f_{J_η}' denote the derivative of f with respect to time and J_η, respectively. Noting that $\mathcal{K}_1 = \Delta_t f\left(n\Delta_t + J_\eta^n\right) + O\left(\Delta_t\right)$, and using (29), J_η^{n+1} in (10) can be arranged as

$$\begin{aligned}J_\eta^{n+1} = & J_\eta^n + (a_1 + a_2)\,\Delta_t f\left(n\Delta_t + J_\eta^n\right) + a_2 \Delta_t^2 \\ & \times \left[\lambda_1 f_t'\left(n\Delta,\, J_\eta^n\right) + \lambda_2 f\left(n\Delta,\, J_\eta^n\right) f_{J_x}'\left(n\Delta,\, J_\eta^n\right)\right] \\ & + O\left(\Delta_t^3\right)\end{aligned} \tag{30}$$

Recalling that J_η^{n+1} can also be written by using the Taylor series expansion as

$$J_\eta^{n+1} = J_\eta^n + \Delta_t J_{\eta_t}' + \frac{\Delta_t^2}{2} J_{\eta_{tt}}'' + O\left(\Delta_t^3\right) \tag{31}$$

and noting that $J_{\eta_t}' = f$ and $J_{\eta_{tt}}'' = f_t' + f_{J_\eta}' f$, (31) can be arranged as

$$\begin{aligned}J_\eta^{n+1} = & J_\eta^n + \Delta_t f\left(n\Delta_t + J_\eta^n\right) + \frac{\Delta_t^2}{2} \\ & \times \left[f_t'\left(n\Delta,\, J_\eta^n\right) + f\left(n\Delta,\, J_\eta^n\right) f_{J_\eta}'\left(n\Delta,\, J_\eta^n\right)\right] \\ & + O\left(\Delta_t^3\right)\end{aligned} \tag{32}$$

Comparing (30) with (32), it can be easily concluded that the explicit RK-FDTD approximation of (10) is of second-order accuracy if

$$a_1 + a_2 = 1, \text{ and } \lambda_1 a_2 = \lambda_2 a_2 = \frac{1}{2} \tag{33}$$

References

1. Geim, K., Novoselov, K.S.: The rise of graphene. Nat. Mater. **6**(3), 183–191 (2007)
2. Taflove, A., Hangess, S.: Computational Electrodynamics: The Finite-Difference Time-Domain Method, 3rd edn. Artech-House, Norwood (2005)

3. Bouzianas, D., Kantartzis, N., Antonopoulos, S., Tsiboukis, T.: Optimal modeling of infinite graphene sheets via a class of generalized FDTD schemes. IEEE Trans. Magn. **48**(2), 379–382 (2012)
4. Bouzianas, G.D., Kantartzis, N.V., Yioultsis, T.V., Tsiboukis, T.: Consistent study of graphene structures through the direct incorporation of surface conductivity. IEEE Trans. Magn. **50**(2), Article no. 7003804 (2014)
5. Papadimopoulos, A.N., Amanatiadis, S.A., Kantartzis, N.V., Rekanos, I.T., Zygiridis, T.T., Tsiboukis, T.D.: A convolutional PML scheme for the efficient modeling of graphene structures through the ADE-FDTD technique. IEEE Trans. Magn. **53**(6), Article no. 7204504 (2017)
6. Fletcher, S.J.: Numerical solutions to initial value problems. In: Data Assimilation for the Geosciences: From Theory to Application, ch. 8, pp. 273–315. Elsevier, U.K. (2017)
7. Ogata, K.: Discrete-Time Control Systems, 2nd edn. Prentice-Hall, New Jersey (1995)
8. Hanson, G.W.: Dyadic Green's functions and guided surface waves for a surface conductivity model of graphene. J. Appl. Phys. **103**(064302) (2008)
9. Vakil, A., Engheta, N.: Transformation optics using graphene. Science **332**(6035), 1291 (2011)
10. Wang, X.H., Yin, W.Y., Chen, Z.: Matrix exponential FDTD modeling of magnetized graphene sheet. IEEE Antennas Wirel. Propag. Lett. **12**, 1129–1132 (2013)
11. Gutschling, S., Kruger, H., Weiland, T.: Time-domain simulation of dispersive media with the finite integration technique. Int J. Numer. Model. **13**, 329–348 (2000)
12. Roden, J.A., Gedney, S.D.: Convolutional PML (CPML): an efficient FDTD implementation of the CFS-PML for arbitrary media. Microw. Opt. Technol. Lett. **27**(5), 334–339 (2000)